Applied Surface Science 370 (2016) 394–402

Contents lists available at ScienceDirect

Applied Surface Science

journal homepage: www.elsevier.com/locate/apsusc

Mechanisms governing the interfacial delamination of thermal barrier coating system with double ceramic layers

Rong Xu, Xueling Fan*, T.J. Wang**

State Key Laboratory for Strength and Vibration of Mechanical Structures, Department of Engineering Mechanics, School of Aerospace Engineering, Xi'an Jiaotong University, Xi'an 710049, China

ARTICLE INFO

Article history:
Received 1 November 2015
Received in revised form 10 February 2016
Accepted 21 February 2016
Available online 23 February 2016

Keywords:
Thermal barrier coating
Delamination
Crack driving force
Finite element method

ABSTRACT

A systematic study of factors affecting the interfacial delamination of thermal barrier coating system (TBCs) with double ceramic layers (DCL) is presented. Crack driving forces for delaminations at two weak interfaces are examined. The results show that a thicker outermost ceramic layer can induce dramatic increase in crack driving force and make the interface between two ceramic coatings become more prone to delamination. The behavior is shown to be more prominent in TBCs with stiffer outmost coating. The thickness ratio of two ceramic layers is an important parameter for controlling the failure mechanisms and determining the lifetime of DCL TBCs under inservice condition. By accounting for the influences of thickness ratio of two ceramic layers and interfacial fracture toughnesses of two involved interfaces, the fracture mechanism map of DCL TBCs has been constructed, in which different failure mechanisms are identified. The results quanlitatively agree with the aviliable experimental data.

1. Introduction

Improving the efficiency of gas turbines is a challenging task for aircrafts as well as power plants. Commonly, efficiency improvement is always associated with the increase of turbine inlet temperature. However, the superalloys currently used for turbine blades have almost reached the limits of their temperature tolerance, thus scientists turn to focus on the technique of thermal barrier coating system (TBCs). TBCs consists of an yttria-partially-stabilized zirconia (YSZ) ceramic top coat (TC), a metallic bond coat (BC), a superalloy substrate, and a protective oxide layer forming during service [1]. Owing to the excellent heat insulating performance of ceramic coating, TBCs can protect gas turbine blades from severe environmental condition through providing a temperature gradient [2,3].

Under extremely high temperature (higher than 1443 K), YSZ TBCs may undergo several significant degradations: sintering, phase change, accelerated oxidation and calcium–magnesium–alumino–silicate (CMAS) deposits. These detrimental processes affect the material properties and microstructure of YSZ TBCs, such as increasing thermal conductivity and Young's modulus, and thus reduce the strain tolerance. A number of literatures reported that the performance and the resilience of YSZ TBCs dramatically drop when operated under extremely high temperature [4–6]. To overcome the remarkable degradations of YSZ TBCs driven by high temperature, scientists are searching for alternative materials with superior low thermal conductivity, high melting point, good resistance to sintering, and long life properties [7]. Cao et al. summarized the basic properties of the advanced ceramic materials [8]. They pointed out that, except YSZ, rare earth oxides such as lanthanum zirconate (LZ) are promising materials for advanced TBCs. However, the coefficients of thermal expansion (CTE) and fracture toughnesses of the candidate materials are much lower than traditional YSZ. Under thermal loading, a field of stress would be induced in coatings due to the huge CTE mismatch, which promotes the mechanical degradation in TBCs. Therefore, rare earth oxides TBCs such as LZ commonly appear a premature failure as well as a short life during service.

Recently, double ceramic layer (DCL) TBCs combining the advantages of YSZ ceramic and its candidate materials becomes a nature choice. The inner YSZ ceramic layer deposited on BC layer is used to reconcile the mismatch of CTE and fracture toughness between outermost layer and substrate superalloy, while the outermost layer with excellent thermal stability protects the inner ceramic layer from sintering, phase change and CMAS penetration. Previous studies have shown that the new DCL design is able to effectively improve the thermal stability and prolong the TBCs life.

* Corresponding author.
** Corresponding author.
E-mail addresses: fanxueling@mail.xjtu.edu.cn (X. Fan), wangtj@mail.xjtu.edu.cn (T.J. Wang).

http://dx.doi.org/10.1016/j.apsusc.2016.02.180
0169-4332/

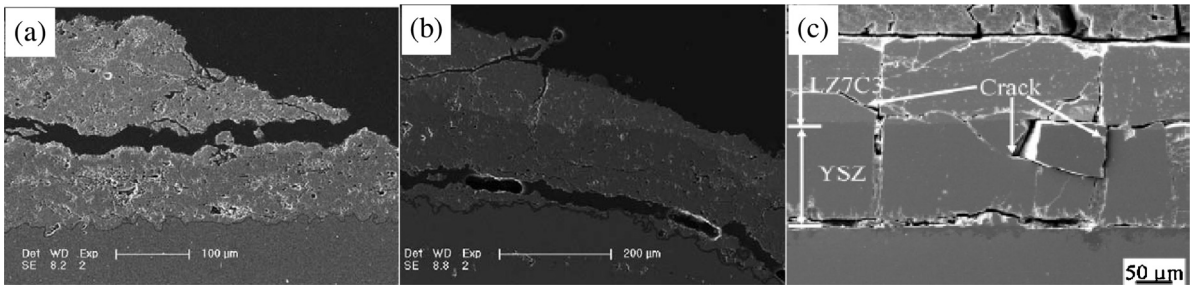

Fig. 1. Dominate failure mechanisms of DCL TBCs: (a) Interface cracks at LZ/YSZ interface. (b) Interface cracks at YSZ/BC interface. Reproduced with permission from Dai, et al. Materials Science and Engineering: A, 433, 2006 by the Elsevier Limited. (c) Multiple surface cracks as well as interface cracks at LZ/YSZ and YSZ/BC interfaces. Reproduced with permission from Xu, et al. Journal of Alloys and Compounds, 509, 2011 by the Elsevier Limited.

The multilayer TBCs usually consists of several phases with a large variation of mechanical properties (i.e. metal, alloy and ceramic layers). During high temperature exposure, different components swell or shrink simultaneously and raise a complex field of stresses. As pointed out by experiment studies, these stresses induce different fracture behaviors within TBCs that can be classified into two major categories: surface crack and interfacial delamination [9–11]. For DCL TBCs, two weak interfaces—the LZ/YSZ interface and the YSZ/BC interface are prone to delamination during service [12,13]. The final failure of TBCs happens by the spallation of ceramic coatings resulting from the propagation and coalescence of interface cracks. Chen et al. observed that the interfacial delamination in DCL TBCs caused by thermal mismatch stress is the essential reason for the failure of DCL TBCs [14]. They modified the interface in DCL TBCs by preparing composite coatings that could decrease the thermal mismatch between YSZ and substrate as well as between LZ and YSZ layers. The modified DCL TBCs exhibited improved strain tolerance and thermal cycling lifetime. Besides the composite coatings, the role of defect at LZ/YSZ interface on the delamination at the YSZ/BC interface was also recognized and analyzed by Fan et al. [15]. Dai et al. conducted the thermal shock experiment to investigate the thermal stability of DCL TBCs with various coating thicknesses [16]. In their studies, different fracture mechanisms were observed in the DCL TBCs with variable coating thickness (i.e., interface cracks at different interfaces, as shown in Fig. 1(a) and (b)). From thermal shock experiments by Xu et al. [17], it is concluded that multiple surface cracks combining with interface cracks at LZ/YSZ and YSZ/BC interfaces dominate the failure of DCL TBCs, as shown in Fig. 1(c). Although different fracture mechanisms were observed in previous studies, a clear understanding of these mechanisms is still missed. Further investigation on the essential incentive of the different fracture mechanisms is needed.

Many previous studies focus on the preparation, characterization, and thermal shock experiment of DCL TBCs [17,18] while relatively little attention has been paid to the failure in DCL TBCs governed by different mechanisms. Basic understanding of the relationship between geometry features and failure mechanisms is of essence for the application of advanced DCL TBCs in gas turbine. The objective of this paper is to investigate the evolution of delamination at the weak interface of LZ/YSZ or YSZ/BC in DCL TBCs. The competitive mechanism between cracks at two different interfaces has been studied by comparing their crack driving forces. From our results, we can predict and control the failure behavior of DCL TBCs by optimal structure design and elaborated deposition processes. In Section 2, we formulate the problem, in which the physical model, the material model and the numerical model are presented. In Section 3, the driving forces for different interface cracks are calculated and the reasons for different fracture mechanisms are discussed. Some concluding remarks are given in Section 4.

2. Formulation of the problem

For typical film/substrate systems under thermal and/or mechanical loading, like TBCs, multiple surface cracking and interfacial delamination are two dominate fracture mechanisms. Usually, mismatch stress firstly induces multiple surface cracks in top layer, which dominates the premature failure of TBCs. After surface cracks reach the underlying interface, interfacial delaminations initiate from roots of surface cracks due to stress singularity, then propagate and coalesce [19–21].

For DCL TBCs, the fracture mechanisms are much complex. On one hand, surface cracks deflect into the LZ/YSZ interface after reaching it. On the other hand, multiple channeling cracks sequentially form and approach to the YSZ/BC interface without kinking into the LZ/YSZ interface. As a result, interface cracks are triggered at the YSZ/BC interface as well. It should be pointed out that throughout this work we use LZ and YSZ to represent the outermost ceramic coat and inner ceramic coat, respectively. Based on previous researches [16,17], multilayer DCL TBCs with surface cracks and interfacial delaminations can be represented graphically as in Fig. 2. Herein, based on experimental observations and theoretical analyses about surface cracking morphologies in film/substrate system [17,22], multiple surface channeling cracks are assumed to periodically distribute in both ceramic coatings. Moreover, those surface cracks reaching the LZ/YSZ interface are assumed to periodically distribute in LZ layer between the channeling cracks in LZ and YSZ layers. In Fig. 2, h_{YSZ} and h_{LZ} represent the thicknesses of LZ and YSZ coatings, respectively, d the length of interface crack and W the spacing between two neighboring surface cracks.

For the multiple cracks in DCL TBC, we consider them as steady-state cracks [22], which means the crack driving force becomes independent of the crack depth once the channeling cracks reach a critical depth along the out-of-plane direction. Thus we simplify the real three-dimensional (3D) DCL TBCs into a two-dimensional (2D) model in Fig. 2(a) and (b). Fig. 2(b) shows the simplified 2D plane strain model of the DCL TBCs with multiple steady-state surface cracks and accompanied interface cracks at LZ/YSZ and YSZ/BC interfaces. Previous studies stated that, for a relatively large crack spacing (roughly larger than twenty times film thickness), the interactions between neighboring cracks can be ignored [20,21]. In this case, the fracture behaviors are only determined by the thickness ratio of LZ to YSZ coating as well as the interface toughness ratio of LZ/YSZ to YSZ/BC interface. To save computation time, the DCL TBCs with cracks at LZ/YSZ and YSZ/BC interfaces can be separated into two cases: DCL TBCs with interface cracks at LZ/YSZ interface and DCL TBCs with YSZ/BC interface cracks, as shown in Fig. 3. We can respectively examine the evolution of interfacial delamination at the LZ/YSZ interface or at the YSZ/BC interface and then clarify the competitive mechanism between two fracture modes. We point out that in this work the spacing between two categories of delamination is assumed to be large enough such that the

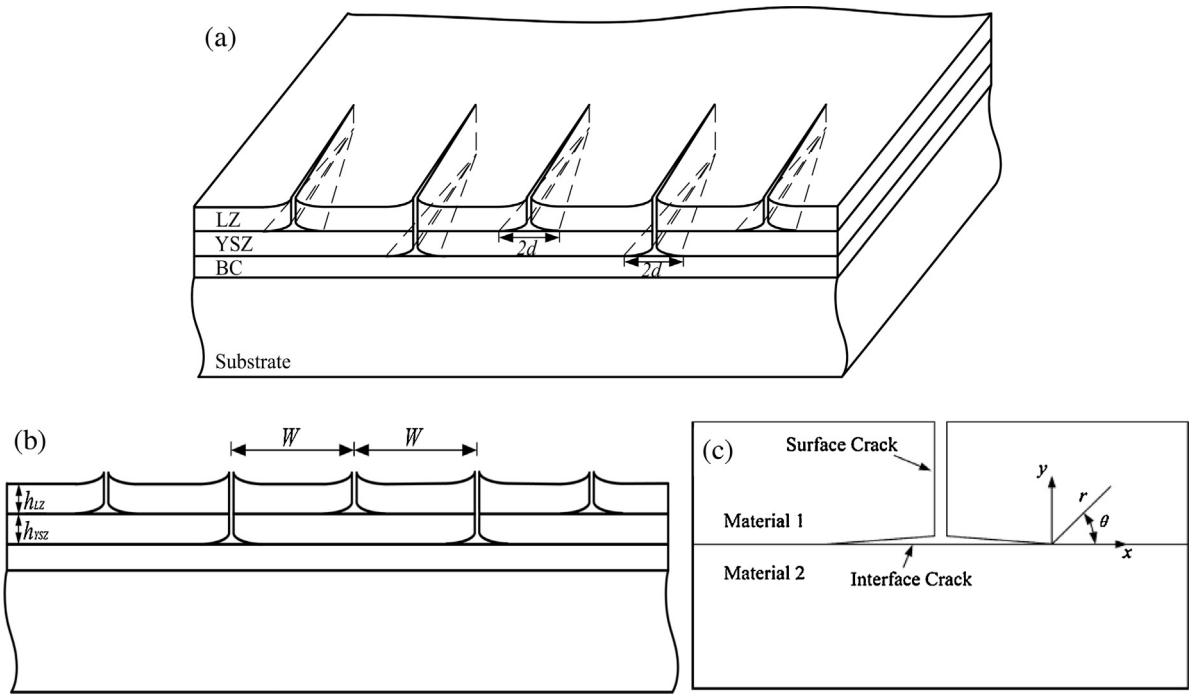

Fig. 2. The geometry of DCL TBCs with multiple surface cracks and interfacial delaminations. (a) The 3D configuration. (b) Simplified 2D model. (c) Geometry and local coordinates of interface cracks initiating from the root of a surface crack.

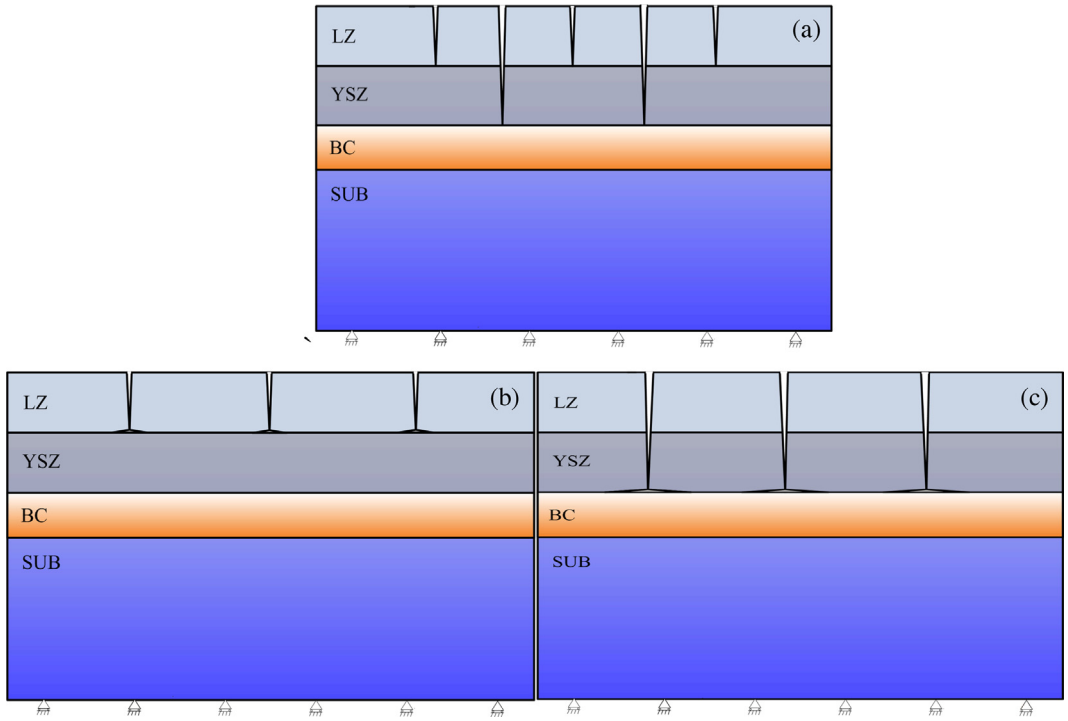

Fig. 3. (a) DCL TBCs with interface cracks at LZ/YSZ interface and YSZ/BC interface. It can be separated into two cases: (b) DCL TBCs with interface cracks at LZ/YSZ interface. (c) DCL TBCs with YSZ/BC interface cracks.

mechanical interaction between interfacial delaminations can be ignored. A previous work provides some discussions on the interactions between the cracks at LZ/YSZ and YSZ/BC interfaces [20,21,23].

In essence, the interfacial delamination in DCL TBCs can be regarded as the bi-material interface crack. Linear elastic fracture mechanic (LEFM) can be used to analysis the evolution of interfacial delamination. In LEFM, the crack flank displacement (δ_1,δ_2) and stress fields $(\sigma_{12},\sigma_{22})$ with a distant r ahead of the interface crack tip can be expressed as

$$\delta_2 + i\delta_1 = \frac{8}{(1+2i\varepsilon)\cosh(\pi\varepsilon)}\frac{K}{E^*}\left(\frac{r}{2\pi}\right)^{1/2} r^{i\varepsilon} \quad (1)$$

$$\sigma_{22} + i\sigma_{12} = K(2\pi r)^{-1/2} r^{i\varepsilon} \quad (2)$$

where $\frac{1}{\bar{E}^*} = \frac{1}{2}\left(\frac{1}{\bar{E}1} + \frac{1}{\bar{E}2}\right)$, $i = \sqrt{-1}$ and $r^{i\varepsilon} = \cos(\varepsilon \ln r) + i\sin(\varepsilon \ln r)$. $\bar{E}_i = E_i/\left(1 - v_i^2\right)$, E_i and $v_i (i = 1, 2)$ are the plane strain modulus, Young's modulus, Poisson's ratio of TBCs components, respectively. The constant ε represents the singularity of crack tip field, which can be defined as $\varepsilon = \frac{1}{2\pi}\ln\frac{1-\beta}{1+\beta}$, where β is the second Dundurs parameter, and K the complex interface stress intensity factor.

The stress concentration near crack tip causes the initiation of interface crack and the subsequent growth. Total elastic energy in the materials decreases as the interface crack advances. The reduction of elastic energy in the material associating with a unit area of crack extension defines the strain energy release rate (SERR) G. In this paper, the SERR is used to stand for the driving force of an interface crack. A larger SERR value at the interface crack tip represents higher probability of interfacial delamination and vice versa. For an interface crack, the SERR can be calculated from Eqs. (1) and (2), as [24]

$$G = \lim_{\Delta a \to 0} \frac{1}{2\Delta a}\int_0^{\Delta a} \boldsymbol{\sigma}(r)\boldsymbol{\delta}(\Delta a - r)dr = \left(\frac{1}{\bar{E}_1} + \frac{1}{\bar{E}_2}\right)\frac{K_1^2 + K_2^2}{2\cosh^2\pi\varepsilon} \quad (3)$$

where K_1 and K_2 are the real and imaginary parts of K and play similar roles to the conventional mode I and model II intensity factors. The mode mixity ψ at a fixed distance ahead of the crack tip is adopted to characterize the relative amount of mode II to mode I fracture at the interface crack tip, which is defined by

$$\psi = \tan^{-1}\left(\frac{\sigma_{12}}{\sigma_{22}}|_{r=l}\right) = \tan^{-1}\left(\frac{Im\,Kl^{i\varepsilon}}{Re\,Kl^{i\varepsilon}}\right) \quad (4)$$

where l is a reference length. To predict the mixed fracture mode of a bi-material system, an in-plane length is preferred.

However, since the stress field at the interface crack tip is relatively complex, it is intractable to calculate the SERR directly. A convenient calculation of SERR is applied in this paper: the energy release associated with crack growth is characterized and calculated by J-integral. On the basis of LEFM, the SERR can be directly relevant to the value of J-integral. For a virtual crack advance $\lambda(s)$, the value of J-integral can be calculated by [25]

$$\bar{J} = \int_A \lambda(s)\, n \cdot \mathrm{H} \cdot q dA \quad (5)$$

where dA is the total areas of a layer of elements enclosing the crack tip, $\boldsymbol{n}$ the outward normal vector to the corresponding integral contour, and $\boldsymbol{q}$ the direction of virtual crack extension, $\boldsymbol{H}$ is given by

$$H = \left(\omega \mathrm{I} - \sigma \cdot \frac{\partial u}{\partial x}\right) \quad (6)$$

where is σ the Cauchy stress tensor, $\boldsymbol{u}$ the displacement vector, and ω the strain energy. For elastic material, ω is the elastic strain energy, while for elastic-plastic or elasto-viscoplastic material, ω is defined as the sum of elastic strain energy and plastic dissipation energy.

In this work, the commercial software ABAQUS is employed for numerical calculation. For the periodic problem illustrated in Fig. 2, periodic boundary condition (P.B.C.) can be adopted to simplify the numerical analysis and reduce the computational effort [26,27]. We suppose the displacements of the nodes allocated on the left and right boundaries satisfy the relation:

$$\begin{cases} u_i\left(-W/2, y\right) - u_0\left(-W/2, 0\right) = u_i\left(W/2, y\right) - u_0\left(W/2, 0\right) \\ v_i\left(-W/2, y\right) - v_0\left(-W/2, 0\right) = v_i\left(W/2, y\right) - v_0\left(W/2, 0\right) \end{cases} \quad (7)$$

where node i is allocated on the left boundary ($x = -W/2$), and node i' allocated on the right side ($x = W/2$). By this way we can ensure the parallel boundaries remain parallel in the tangential sense. A uniform tensile elongation instead of thermal load is applied to the model. Eight-node biquadratic plane strain quadrilateral reduced integration elements are selected for all layers except the crack tip region, where very fine mesh of singular elements are constructed, as shown in Fig. 4. Actually, under real service condition, the thermal expansion induced by the CTE mismatch is a volumetric deformation which would lead to thermal strain and stress in 33-direction. Applying the uniform tensile elongation instead of thermal load ignores the thermal strain in 33-direction which would underestimate the elastic energy stored in this system, as well as the energy release rate during crack propagation. Therefore, considering the horizontal in-plane tension loading coming from the thermal expansion of the substrate may induce a slight difference when compared with the result from the system under the real boundary condition. Mesh sensitivity of the numerical results is examined to ensure that the J contour integral values are independent of the mesh configuration. Elaborate mesh refinement around the crack tip ensures convergent SERR values. Specifically, the first layer of elements enclosed the crack front is used to calculate the first contour integral. Since the first few contour integrals are defined by the nodes close to the crack tip, the values of J integral could be inaccurate. More integral contours are set to obtain the accurate value that is ensured once the values for two adjacent integral contours reach convergence.

A reference DCL TBCs structure is selected as a benchmark. The material properties are presented in Table 1. The initial thicknesses of LZ, YSZ, BC and substrate are assumed to be 50 um, 250 um, 100 um and 3 mm, respectively. The width of the TBC system W is twenty times the total thickness of the ceramic layers. In this case the interactions between neighboring vertical cracks can be ignored. To evaluate the mechanisms governing the interfacial delamination, different geometric properties of outermost ceramic layer have been considered, where the thickness of LZ layer varies from 50 to 250 um while the total thickness of two ceramic layers remains constant.

3. Results and discussions

During services, interface cracks appear simultaneously or sequentially at the LZ/YSZ and YSZ/BC interfaces. Herein, we focus on the competitive mechanism between the interfacial delaminations at the two interfaces. Specifically, we numerically analyze the crack driving force (i.e., SERR) of interface cracks, and then construct a failure map through systematic analysis. By this way, we can provide practical guidance for predicting and controlling the fracture mechanisms in DCL TBCs.

Commonly, the thickness ratio of LZ to YSZ layers has a significant influence on the stored energy within the system, also the crack driving force for delamination. The effects of the relative thickness of two ceramic layers on the SERR values of delaminations at the LZ/YSZ and YSZ/BC interfaces are discussed herein. Fig. 5(a) presents the SERR as a function of the normalized delamination length d/h_f at the YSZ/BC interface for different thickness ratios of two ceramic layers. The evolution of SERR in Fig. 5(a) indicates that an oscillation exists at the beginning of the propagation of interfacial delamination. The SERR would dramatically increase from zero to the maximum value G_{max} during the initiation of the interfacial delamination, and then drops to the steady state. The G_{max} value is critical to estimate the emanation of the delamination. Interface cracks do not advance unless the G_{max} is greater than or equal to the interfacial fracture toughness. As the crack keeps growing along the interface, SERR declines until a steady-state is reached. During this stage, SERR becomes independent of the interfacial delamination length, and then stays at the steady state G_{ss} that represents

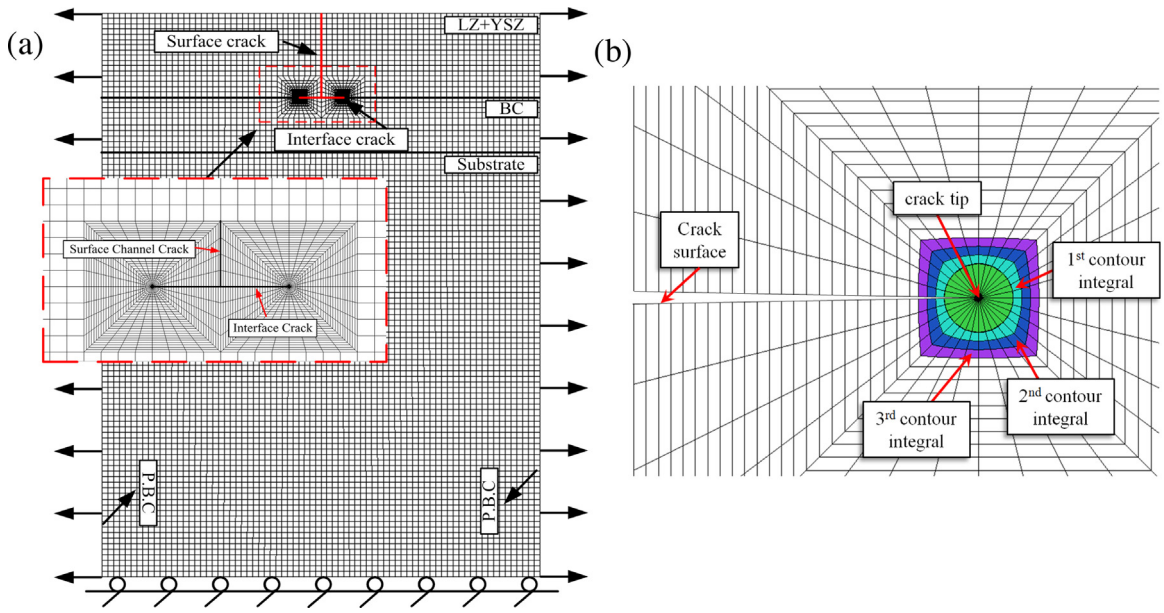

Fig. 4. (a) Finite element model of DCL TBCs with surface crack and interface cracks. (b) Characteristic of the contour integrals around an interface crack tip.

Table 1
Material properties of the DCL-TBCs.

	Outermost ceramic coating	Inner ceramic coating	Bond coat	Substrate
Young's modulus (GPa)	120	60	200	211
Poisson ratio	0.25	0.1	0.3	0.3

the driving force for the stable extension of delamination. Note that the SERR evolution of delamination at the YSZ/BC interface coincides with the evolution of driving force of interface crack in film/substrate system with soft film and stiff substrate [21,27]. The similarity is a result of the combination of a softer YSZ upper layer and a stiffer BC lower layer.

Fig. 5(b) shows the variation of SERR as a function of the delamination length at the LZ/YSZ interface for various thickness ratios of two ceramic layers. Different with the SERR evolution of delamination at the YSZ/BC interface, a monotone trend is observed. Due to the relatively high elastic energy stored in the stiffer LZ layer, SERR stays at high level even for short interface cracks. Then it drops to a stable, lower level value as the crack propagates. The evolution of SERR of delamination at the LZ/YSZ interface is qualitatively in accord with the SERR evolution of interface crack in stiff film/compliant substrate systems [27]. In Fig. 5(a) and (b), it is concluded that a higher thickness ratio of h_{LZ}/h_{YSZ} induces larger SERR values (including G_{max} and G_{ss}) for both LZ/YSZ and YSZ/BC interface cracks. Thus the initiation and propagation of interfacial delaminations at two interfaces would be triggered more easily. It may well explain why the lifetime of DCL TBCs with a thicker LZ layer is often shorter than that of with a thinner LZ layer [16].

The reason why SERR would be enlarged by increasing the thickness of LZ layer can be further explained through analyzing the elastic energy stored in the ceramic layers. When increasing the thickness of the stiffer outmost layer (e.g., LZ layer with 120 GPa Young's modulus), the total elastic energy stored in two ceramic layers is enlarged even though the total thickness of the ceramic layers still remains the same. It would dramatically raise the driving force of the crack at YSZ/BC interface, as shown in Fig. 5(a). However, if considering the Young's modulus of outmost layer as same as that of inner layer (e.g., setting the Young's modulus of LZ layer as 60 GPa), the total elastic energy in two ceramic layers would not be affected by different thickness ratios. In this case, the driving force for the YSZ/BC interface crack is independent of the thickness ratio, as shown in Fig. 5(c). However, the SERR of the LZ/YSZ interface crack is still affected by the thickness ratio of two ceramic layers even with same property. It should be noted that in this case the SERR depends on the elastic energy stored in the LZ layer instead of that in two ceramic layers. We know this part of elastic energy is strongly affected by the thickness of LZ layer. Therefore, we can find in Fig. 5(d) the driving force of the interface crack between two ceramic layers with same property would rise as the thickness ratio increases. Certainly, due to the low stiffness of LZ layer, this influence of the thickness change is less obvious when compared with the result in Fig. 5(b).

Since the effects of relative thickness h_{LZ}/h_{YSZ} on delaminations at the LZ/YSZ and YSZ/BC interfaces are similar, it is difficult to explicitly clarify the governing mechanisms for interfacial fracture in DCL TBCs from the evolution of SERR in Fig. 5. According to LEFM, crack driving force (i.e., SERR or G) as well as interface fracture toughness Γ work together to determine the fracture behavior of interfacial delamination. Therefore, interface fracture toughness Γ should be considered to examine the fracture behavior in DCL TBCs. The interface fracture toughness Γ at LZ/YSZ or YSZ/BC interfaces can be dramatically affected by the deposit process like different ceramic powder and deposit velocity [28,29]. Accurate values of Γ are commonly not available in literature or manual. Herein, we assume the facture toughness Γ at the LZ/YSZ and YSZ/BC interfaces varies over a wide range considering various deposit processes and ceramic powders.

In the case of two involved interfaces with same fracture toughness (i.e. the interface fracture toughness ratio $\Gamma_{LZ/YSZ}/\Gamma_{YSZ/BC}$ equals to 1), the investigation of fracture mechanism competing in DCL TBCs can be simplified by comparing the SERR of delamination at LZ/YSZ interface with that of at YSZ/BC interface. Fig. 6(a) shows the SERR evolutions of delaminations at the LZ/YSZ and YSZ/BC interfaces for $h_{LZ}/h_{YSZ} = 0.2$, in which the red line stands for the

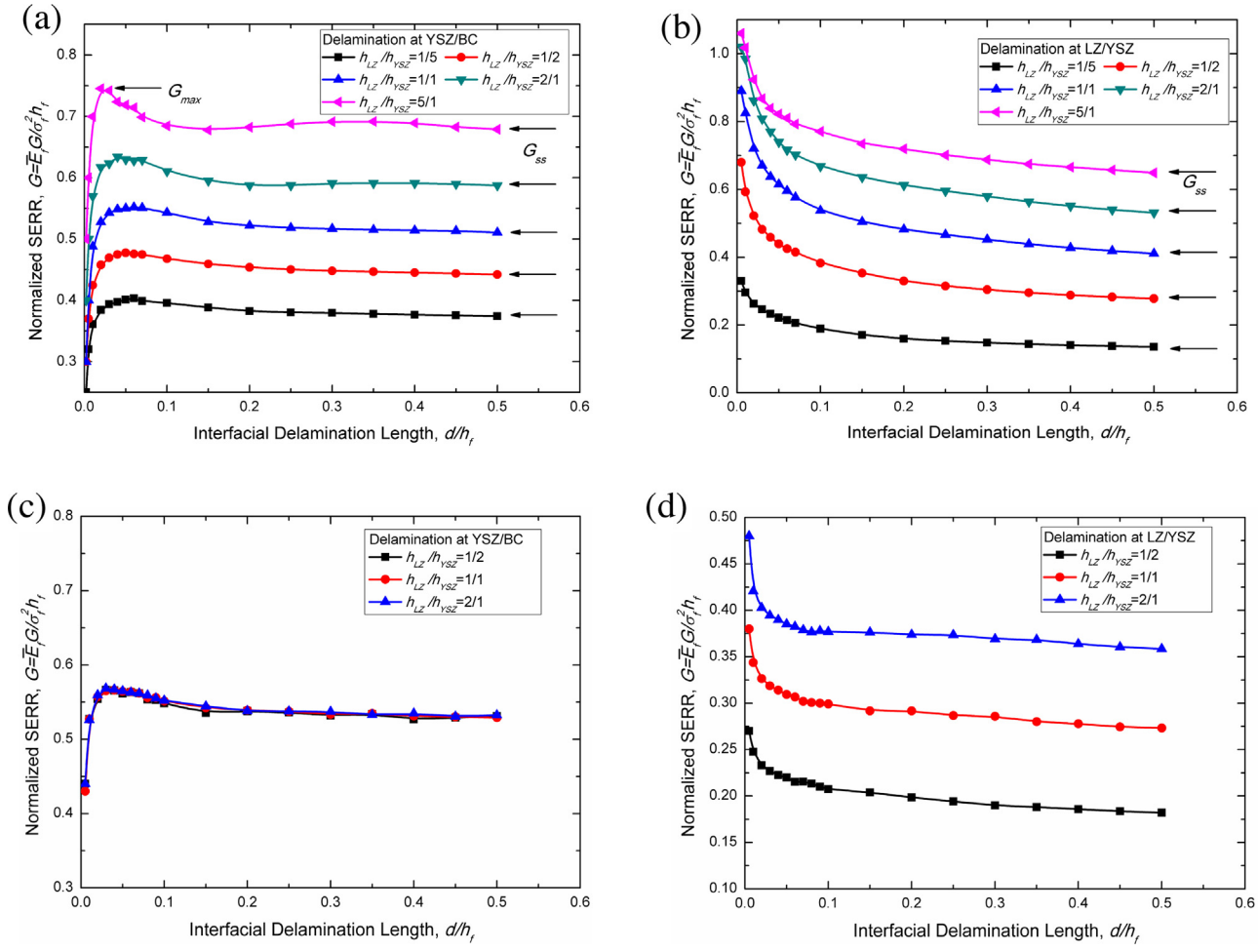

Fig. 5. SERR as a function of delamination length at (a) the LZ/YSZ interface and (b) the YSZ/BC interface for different thickness ratios of two different ceramic layers. SERR as a function of delamination length at (c) the LZ/YSZ interface and (d) the YSZ/BC interface for different thickness ratios of two identical ceramic layers.

SERR of the delamination at YSZ/BC interface (i.e., $G_{YSZ/BC}$) while the black line stands for the SERR of the delamination at LZ/YSZ interface (i.e., $G_{LZ/YSZ}$). We can notice that except at the early stage, $G_{YSZ/BC}$ is always larger than $G_{LZ/YSZ}$, which indicates that in case of $\Gamma_{LZ/YSZ}/\Gamma_{YSZ/BC}=1$ and $h_{LZ}/h_{YSZ}=0.2$, the delamination at YSZ/BC interface dominates the fracture of DCL TBCs. The final failure of DCL TBCs manifests as the spallation of both two ceramic coating layers, which results in the exposure of substrate superalloy to extreme high temperature enviroments.

Keeping the interface fracture toughness ratio fixed and varying the ceramic layer thickness ratio from 1 to 5, we can obtain the corresponding SERR evolutions of the delaminations at the LZ/YSZ and YSZ/BC interfaces in Fig. 6(b) and (c). In Fig. 6(b), we notice that after reaching the steady state, $G_{YSZ/BC}$ is comparable with $G_{LZ/YSZ}$, indicating that, for DCL TBCs with $\Gamma_{LZ/YSZ}/\Gamma_{YSZ/BC}=1$ and $h_{LZ}/h_{YSZ}=1.0$, the final fracture mechanism appears to be a combination of delaminations at the LZ/YSZ as well as YSZ/BC interfaces. Increasing the thickness ratio of two ceramic layers until it reaches up to 5, we observe both $G_{LZ/YSZ}$ and $G_{YSZ/BC}$ grow, as shown in Fig. 6(c). However, $G_{LZ/YSZ}$ rises more rapidly than $G_{YSZ/BC}$. This behavior infers that the delamination at the LZ/YSZ interface are more likely to dominate the fracture of DCL TBCs with a thicker LZ layer. As expected, it will induce another failure mode in DCL TBCs—LZ layer spalls while YSZ layer keeps attaching to the underlying BC layer.

As stated above, the SERR G and the interface fracture toughness Γ work together to govern the cracking behavior. When G/Γ reaches to 1, crack is assumed to initiate and propagagte. Herein, we focus the comtribution of relative value of $\Gamma_{LZ/YSZ}$ and $\Gamma_{YSZ/BC}$ on the competitive mechanism of delaminations at the LZ/YSZ and YSZ/BC interfaces. We calculate the SERR ratio of cracks at the two interfaces, $G_{LZ/YSZ}/(G_{YSZ/BC})_{max}$, and then compare them with the interface fracture toughness ratio $\Gamma_{LZ/YSZ}/\Gamma_{YSZ/BC}$. When $G_{LZ/YSZ}/(G_{YSZ/BC})_{max} > \Gamma_{LZ/YSZ}/\Gamma_{YSZ/BC}$, or reformulation as: $G_{LZ/YSZ}/\Gamma_{LZ/YSZ} > (G_{YSZ/BC})_{max}/\Gamma_{YSZ/BC}$, $G_{LZ/YSZ}/\Gamma_{LZ/YSZ}$ satisfies the failure criterion firstly. The interface crack always first appears at the LZ/YSZ interface. We regard the relationship $G_{LZ/YSZ}/(G_{YSZ/BC})_{max} > \Gamma_{LZ/YSZ}/\Gamma_{YSZ/BC}$ as a precondition for the fracture mechanism dominated by delamination at the LZ/YSZ interface. This approach has been used succesfully in many materials and structures, such as thin films [22], composites [30], and ploycrystals [31].

In Fig. 7, solid lines represent the relative SERR values $G_{LZ/YSZ}/(G_{YSZ/BC})_{max}$ for two interface cracks. The dash lines stand for assumed interface fracture toughness ratios $\Gamma_{LZ/YSZ}/\Gamma_{YSZ/BC}$. For those regions that a solid line lies above a dashed line, also $G_{LZ/YSZ}/(G_{YSZ/BC})_{max} > \Gamma_{LZ/YSZ}/\Gamma_{YSZ/BC}$, the delamination at LZ/YSZ interface appears first and dominates the failure of DCL TBCs. In Fig. 7, we find that for DCL TBCs with $h_{LZ}/h_{YSZ}=0.2$, the solid line $G_{LZ/YSZ}/(G_{YSZ/BC})_{max}$ is mostly below the dashed line $\Gamma_{LZ/YSZ}/\Gamma_{YSZ/BC}=1$. Therefore, the delamination at the YSZ/BC dominates the failure of DCL TBCs. On the contrary, $G_{LZ/YSZ}/(G_{YSZ/BC})_{max}$ for DCL TBCs with $h_{LZ}/h_{YSZ}=2.0$ is mostly larger than $\Gamma_{LZ/YSZ}/\Gamma_{YSZ/BC}=1$. In this case, the dominant failure mode of DCL TBCs is delamination at the LZ/YSZ interface. These results

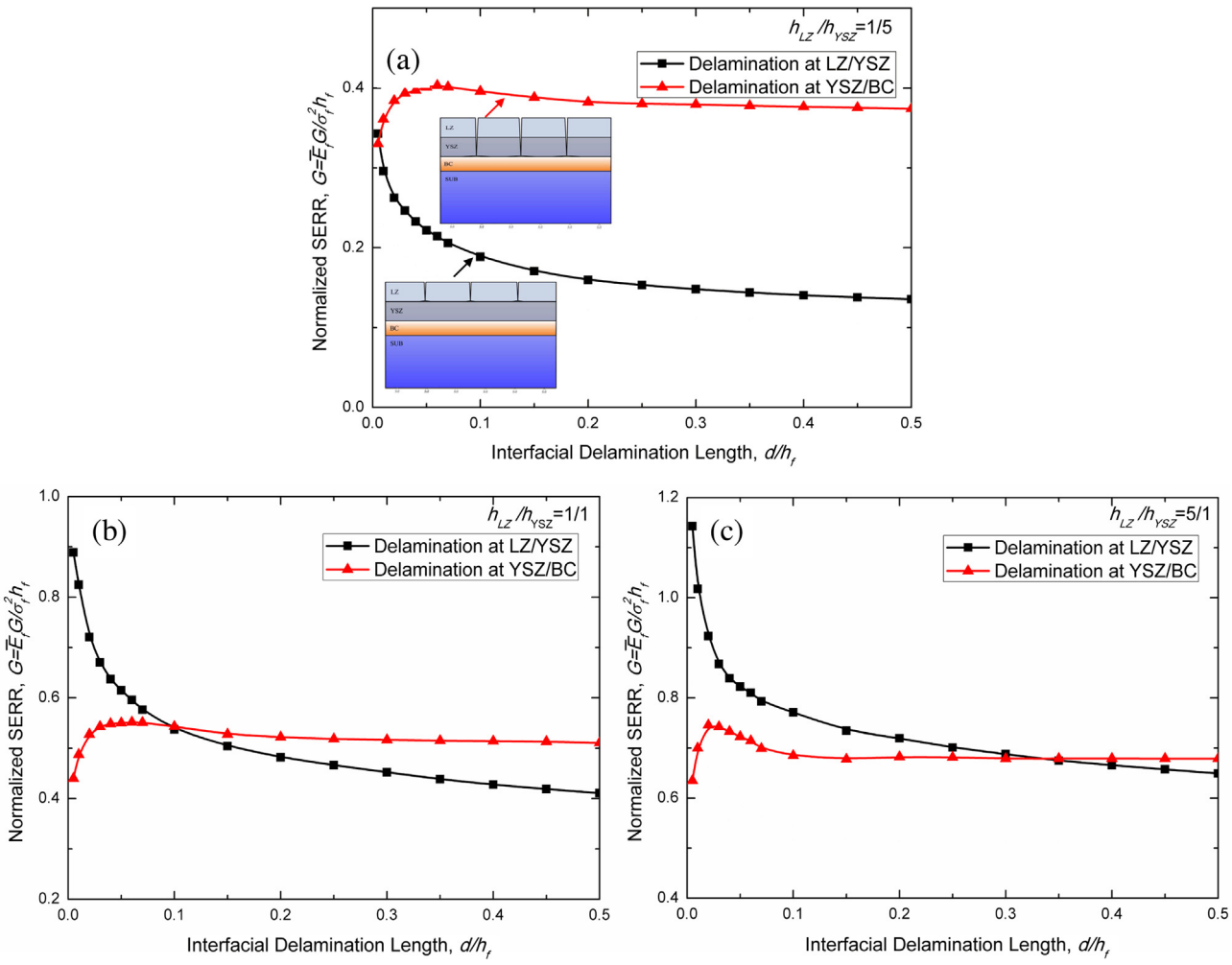

Fig. 6. The SERR evolutions of delaminations at the LZ/YSZ and theYSZ/BC interfaces for DCL TBCs with different thickness ratios:(a) h_{LZ}/h_{YSZ} = 1/5; (b) h_{LZ}/h_{YSZ} = 1/1; (c) h_{LZ}/h_{YSZ} = 5/1.

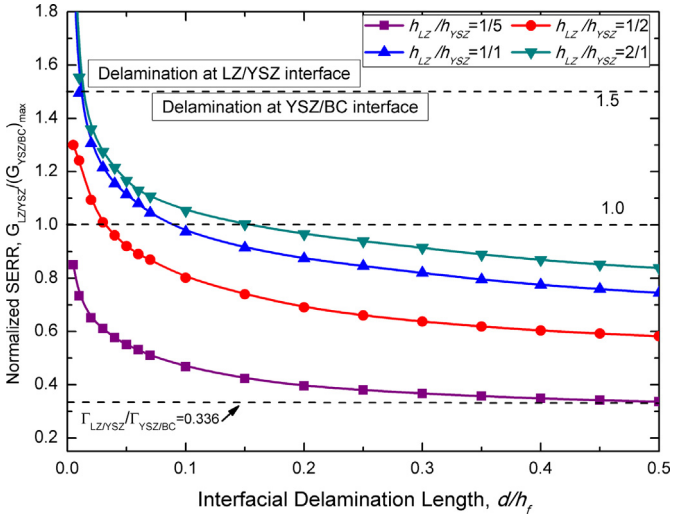

Fig. 7. Relative SERR ratio $G_{LZ/YSZ}/(G_{YSZ/BC})_{max}$ as a function of delamination length for different thickness ratios of two ceramic layers.

agree with the conclusions from Fig. 6. Moreover, we notice that a horizontal asymptote alway exists for each solid line in Fig. 7. It means a critical interface fracture toughness ratio exists, enabling the fracture to occur at the LZ/YSZ interface only. For example, for the DCL TBCs with h_{LZ}/h_{YSZ} = 0.2, if the interface fracture toughness ratio $\Gamma_{LZ/YSZ}/\Gamma_{YSZ/BC}$ is smaller than 0.336, the fracture mechanism is dominated by the LZ/YSZ interface delamination. As a result, the final failure of the DCL TBCs is spallation of LZ layer while YSZ layer keeps intact.

Through caculating a series of horizontal asymptotes for each solid line presented in Fig. 7, we can obtain the boundry for different fracture mechanisms and thus the fracture mechanism map can be constructed, as shown in Fig. 8. As mentioned above, the black line is obtained from Fig. 7 while the red line comes from the calculations of $(G_{LZ/YSZ})_{max}/G_{YSZ/BC}$ and $\Gamma_{LZ/YSZ}/\Gamma_{YSZ/BC}$ by the similar approach. Note that the $(G_{LZ/YSZ})_{max}$ is the maximum SERR value in Fig. 5 for relatively short interfacial delamination (the length is comparable with the size of interface flaw). The black line and the red line allow us to give the boundries of fracture mechanisms dominated by the delaminations at the LZ/YSZ and/or YSZ/BC interfaces, respectively. The region between two boundries is chracterized by a combination of delaminations occurs at two different interfaces simutaneously. As a consequence, the fracture mechanisms in Fig. 8 can be classified into three categories: delamination at the LZ/YSZ interface, at the YSZ/BC interface and delaminations simutaneously appear at the LZ/YSZ and YSZ/BC interfaces. In Fig. 8, the fracture mechanism is dominated by delamination at the LZ/YSZ interface for low fracture toughness ratio and high thickness ratio. With the increase of the fracture toughness ratio and/or the decrease of the thickness ratio, the YSZ/BC interface becomes prone to debond,

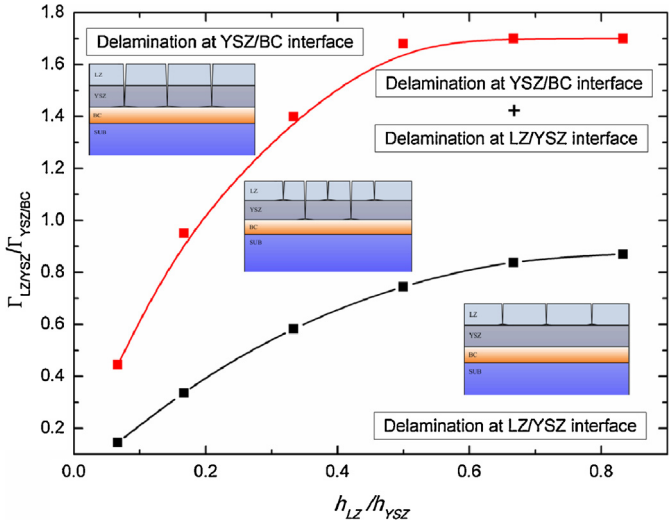

Fig. 8. Fracture mechanisms in DCL TBCs with different thickness ratios and interface fracture toughness ratios.

resulting in the mixed fracture mechanism. For high fracture toughness ratio and/or low thickness ratio, delamination at the YSZ/BC interface can be easily formed in the failure process of DCL TBCs. These numerical results quanlitatively agree with the experimental observations of Dai et al. [16]. Their experiments also shown that higher thickness ratio of LZ to YSZ layers mainly induces the fracture at the LZ/YSZ interface while lower thickness ratio is more likely to induce failure at the YSZ/BC interface. Meanwhile, the different fracture mechanims obtained by Dai et al. can be fitted well into our fracture mechanism map.

In fact, although three fracture zones are numerically identified in Fig. 8, it is believed that in practical applications of TBCs, delamination at the YSZ/BC interface can seldom be observed. This fracture mechanism requires low thickness ratios and high fracture toughness ratios. For relatively low thickness ratio, as shown in Fig. 5, the driving force of interface crack is small, probably lower than the fracture toughness. In this case, interface crack can hardly be triggered at the YSZ/BC interface. Moreover, a high fracture toughness ratio also means a high fracture toughness of LZ/YSZ interface. It is seldom the case for currently well adopted deposition technique. Thus the fracture toughness of LZ/YSZ interface is often limited to a relatively low value. Based on these considerations, the fracture mechanism of DCL TBCs is mainly governed by the delamination at the LZ/YSZ interface, and less by the delamination at the YSZ/BC interface.

4. Conclusion

A basic understanding of the failure mechnisms in complex multi-layer thermal barrier coating system (TBCs) is essential for improving its performance and durability. In this paper, the cracking behaviors of the delaminations at the interfaces between outmost ceramic coat and inner ceramic coat and between the inner ceramic coat and bond coat have been investigated through the examing of their crack driving forces. We discuss the competitive failure mechanism between two interfaces and construct the fracture mechanism map for double ceramic layer (DCL) TBCs.

It is concluded that the interface cracking in DCL TBCs is significantly affected by the thickness ratio of two ceramic coatings. A higher thickness ratio, like a thicker, stiffer outmost ceramic coating with a thinner, compliant inner ceramic layer, may induce a larger crack driving force. As a result, the delaminations at two weak interfaces may be trigged easily. Also, for DCL TBCs with a relatively thick, stiff outermost ceramic layer, the interface between two ceramic layers is more prone to fracture, and thus the outmost ceramic layer easily spalls while the inner ceramic layer keeps attaching to the underlying bond coat layer.

Further investigations reveal that the thickness ratio of two ceramic layers as well as the toughness ratio of two weak interfaces codetermine the fracture mechanism in DCL TBCs. The failure map can be obtained based on parametric investigations of the dependences of fracture behaviors on the geometrical and material properties. In the fracture mechanism map, it appears that cracks will form at the interface of two ceramic layers if the DCL TBCs has a thick, stiff outmost layer and a low interface fracture toughness at the interface of two ceramic layers. The numerical results can explain some failure phenomenons observed in experiments, and provide some design criterions for improving the performance and durability of advanced TBCs.

Acknowledgments

This work is supported by China 973 Program (2013CB035700) and National Natural Science Foundation of China (11472204, 11272259, 11321062 and 11172227).

References

[1] R. Swadźbaa, M. Hetmańczykb, J. Wiedermanna, L. Swadźbab, G. Moskal, B. Witala, K. Radwański, Microstructure degradation of simple: Pt– and Pt+ Pd–modified aluminide coatings on CMSX-4 superalloy under cyclic oxidation conditions, Surf. Coat. Technol. 215 (2013) 16–23.
[2] R.A. Miller, Current status of thermal barrier coatings—an overview, Surf. Coat. Technol. 30 (1987) 1–11.
[3] N.P. Padture, M. Gell, E.H. Jordan, Thermal barrier coatings for gas-turbine engine applications, Science 296 (2002) 280–284.
[4] R.A. Miller, C.E. Lowell, Failure mechanisms of thermal barrier coatings exposed to elevated temperatures, Thin Solid Films 95 (1982) 265–273.
[5] X. Cao, R. Vassen, W. Fischer, F. Tietz, W. Jungen, D. Stoever, Lanthanum–cerium oxide as a thermal barrier coating material for high temperature applications, Adv. Mater 15 (2003) 1438–1442.
[6] R. Xu, X.L. Fan, W.X. Zhang, T.J. Wang, Interfacial fracture mechanism associated with mixed oxides growth in thermal barrier coating system, Surf. Coat. Technol. 253 (2014) 139–147.
[7] D. Clarke, C. Levi, Materials design for the next generation thermal barrier coatings, Annu. Rev. Mater. Res. 33 (2003) 383–417.
[8] X. Cao, R. Vassen, D. Stoever, Ceramic materials for thermal barrier coatings, J. Eur. Ceram. Soc. 24 (2004) 1–10.
[9] R.B. Wei, K. Zhou, L.M. Keer, Q. Fan, Modeling surface pressure: interfacial stresses and stress intensity factors for layered materials containing multiple cracks and inhomogeneous inclusions under contact loading, Mech. Mater. 92 (2016) 8–17.
[10] S. Ahmadian, A. Browning, E.H. Jordan, Three-dimensional X-ray micro-computed tomography of cracks in a furnace cycled air plasma sprayed thermal barrier coating, Scr. Mater. 97 (2015) 13–16.
[11] T.J. Wang, Unified CDM model and local criterion for ductile fracture—I: unified CDM model for ductile fracture, Eng. Fract. Mech. 42 (1992) 177–183.
[12] M. Han, G. Zhou, J. Huang, S. Chen, A parametric study of the double-ceramic-layer thermal barrier coatings part I: optimization design of the ceramic layer thickness ratio based on the finite element analysis of thermal insulation (take LZ_7C_3/8YSZ/NiCoAlY DCL-TBC for an example), Surf. Coat. Tech. 236 (2013) 500–509.
[13] M. Han, J. Huang, S. Chen, A parametric study of the Double-Ceramic-Layer Thermal Barrier Coating Part II: optimization selection of mechanical parameters of the inside ceramic layer based on the effect on the stress distribution, Surf. Coat. Tech. 238 (2014) 93–117.
[14] X.L. Chen, Y. Zhao, X.Z. Fan, Y.J. Liu, B.L. Zou, Y. Wang, H.M. Ma, X. Cao, Thermal cycling failure of new LaMgAl11O19YSZ double ceramic top coat thermal barrier coating systems, Surf. Coat. Tech 205 (2011) 3293–3300.
[15] X.L. Fan, R. Xu, T.J. Wang, Interfacial delamination of double-ceramic- layer thermal barrier coating system, Ceram. Int. 40 (2014) 13793–13802.
[16] H. Dai, X.H. Zhong, J.Y. Li, Y.F. Zhang, J. Meng, X. Cao, Thermal stability of double-ceramic-layer thermal barrier coatings with various coating thickness, Mater. Sci. Eng. A 433 (2006) 1–7.
[17] Z.H. Xu, S.M. He, L.M. He, R.D. Mu, G.H. Huang, X. Cao, Novel thermal barrier coatings based on $La_2(Zr_{0.7}Ce_{0.3})_2O_7$/8YSZ double-ceramic-layer systems deposited by electron beam physical vapor deposition, J. Alloys Compd. 236 (2011) 500–509.
[18] X.H. Zhong, H.Y. Zhao, X.M. Zhou, C.G. Liu, L. Wang, F. Shao, K. Yang, S.Y. Tao, C.X. Ding, Thermal shock behavior of toughened gadolinium zirconate/YSZ

double-ceramic-layered thermal barrier coating, J. Alloys Compd. 593 (2014) 50–55.
[19] L. Yang, Y.C. Zhou, W.G. Mao, C. Lu, Real-time acoustic emission testing based on wavelet transform for the failure process of thermal barrier coatings, Appl. Phys. Lett. 93 (2008) 231906.
[20] X.L. Fan, R. Xu, W.X. Zhang, T.J. Wang, Effect of periodic surface cracks on the interfacial fracture of thermal barrier coating system, Appl. Surf. Sci. 258 (2012) 9816–9823.
[21] R. Xu, X.L. Fan, W.X. Zhang, Y. Song, T.J. Wang, Effects of geometrical and material parameters of top and bond coats on the interfacial fracture in thermal barrier coating system, Mater. Des. 47 (2013) 566–574.
[22] J. Hutchinson, Z. Suo, Mixed mode cracking in layered materials, Adv. Appl. Mech. 29 (1992) 63–191.
[23] X.L. Fan, W. Jiang, J.G. Li, T. Suo, T.J. Wang, R. Xu, Numerical study on interfacial delamination of thermal barrier coatings with multiple separations, Surf. Coat. Tech. 244 (2014) 117–122.
[24] M.Y. He, J.W. Hutchinson, Crack deflection at an interface between dissimilar elastic materials, Int. J. Solids Struct. 25 (1989) 1053–1067.
[25] ABAQUS User's Manual, Dassault Systèmes Simulia Corporation, 2009.
[26] W.X. Zhang, T.J. Wang, L.X. Li, Numerical analysis of the transverse strengthening behavior of fiber-reinforced metal matrix composites, Comput. Mater. Sci. 39 (2007) 684–696.
[27] T. Ye, Z. Suo, A.G. Evans, Thin film cracking and the roles of substrate and interface, Int. J. Solids Struct. 29 (1992) 2639–2648.
[28] P.F. Zhao, C.A. Sun, X.Y. Zhu, F.L. Shang, C.J. Li, Fracture toughness measurements of plasma-sprayed thermal barrier coatings using a modified four-point bending method, Surf. Coat. Technol. 204 (2010) 4066–4074.
[29] G. Qian, T. Nakamura, C.C. Berndt, S.H. Leigh, Tensile toughness test and high temperature fracture analysis of thermal barrier coatings, Acta Mater. 45 (1997) 1767–1784.
[30] T.C. Lu, J. Yang, Z. Suo, A.G. Evans, R. Hecht, R. Mehrabian, Matrix cracking in intermetallic composites caused by thermal expansion mismatch, Acta Metall. Mater. 39 (1991) 1883–1890.
[31] F. Ghahremani1, J.W. Hutchinson1, V. Tvergaard, Three-dimensional effects in microcrack nucleation in brittle Polycrystals, J. Am. Ceram. Soc. 73 (1990) 1548–1554.